Chemical Science

Accepted Manuscript

This article can be cited before page numbers have been issued, to do this please use: X. Sun, Q. Xue, Z. Zhu, Q. Xiao, K. Jiang, H. Yip, H. Yan and Z. Li, *Chem. Sci.*, 2018, DOI: 10.1039/C7SC05484J.

ROYAL SOCIETY OF CHEMISTRY

rsc.li/chemical-science

View Article Online
DOI: 10.1039/C7SC05484J

Journal Name

ARTICLE

Fluoranthene-based Dopant-free Hole Transporting Materials for Efficient Perovskite Solar Cells

Received 00th January 20xx,
Accepted 00th January 20xx

DOI: 10.1039/x0xx00000x

www.rsc.org/

Xianglang Sun,[a†] Qifan Xue,[c†] Zonglong Zhu,*[b] Qi Xiao,[a] Kui Jiang,[b] Hin-Lap Yip,[c] He Yan*[b] and Zhong'an Li*[a]

Significant efforts have been denoted on developing new dopant-free hole transporting materials (HTMs) for perovskite solar cells (PVSCs). Fluoranthene is one typical cyclopentene-fused polycyclic aromatic hydrocarbon with rigid planarized structure, and thus could be an ideal building block to construct dopant-free HTMs, which, however, has not been reported yet. Here, we report a new and simple synthetic method to prepare unreported 2,3-dicyano-fluoranthene though a Diels-Alder reaction between dibenzofulvene and tetracyanoethylene, and demonstrate it can serve as efficient electron-withdrawing unit for constructing donor-acceptor (D-A) type HTMs. This novel building block not only endows the resulting molecules with suitable energy levels, but also enables highly ordered and strong molecular packing in solid states, both of which could facilitate the hole extraction and transport. Thus as dopant-free HTMs, impressive efficiencies of 18.03% and 17.01% associated with enhanced stability can be achieved based on conventional n-i-p and inverted p-i-n PVSCs, respectively, outperforming most organic dopant-free HTMs reported so far.

Introduction

Organic-inorganic hybrid perovskite solar cells (PVSCs) have triggered a worldwide attention due to their impressive research progress within a short time and very promising market prospects.[1-5] Recently, the record-high power conversion efficiency (PCE) of PVSCs has reached the certified 22%, almost rivaling that of the crystalline silicon based photovoltaics.[6] When fabricating PVSCs, the introduction of suitable interfacial materials, i.e. electron transporting materials (ETMs) and hole transporting materials (HTMs), is very critical to achieve high device performance, because they not only improve the charge carrier transport/collection efficiency, but also act as the protective layer for perovskites to enhance device stability.[7-11]

For HTMs applied on PVSCs, organic semiconductors are more popular over inorganic counterparts attributed to their milder processing conditions compatible with perovskites. Nevertheless, most organic HTMs exhibit relatively low hole mobility, and thus needs to be improved through a chemical doping process by ionic dopants such as Li-bis(trifluoromethanesulfonyl)imide (Li-TFSI).[12-16] However, doping process always induces a negative effect on device stability due to the sophisticated oxidation process associated with undesired ion migration/interactions.[17, 18] For example, the device PCEs derived from well-known doped HTM, 2,2',7,7'-tetrakis(*N,N*-bis(p-methoxyphenyl)amino)-9,9'-spirobifluorene (spiro-OMeTAD), often vanished after 30-day ambient storage, even the maximum of its initial PCEs has been close to 19%.[19] Thus, development of efficient dopant-free HTMs is urgently needed, however less dopant-free HTMs can show comparable PCEs to the doped spiro-OMeTAD.[18, 20-26]

Normally, HTMs would not need an additional doping process if they exhibit hole mobility up to 10^{-4}~10^{-3} $cm^2V^{-1}s^{-1}$.[27] To this end, two molecular design strategies, donor-acceptor (D-A) type and star-shaped structure, have been mainly used for designing dopant-free HTMs with better intermolecular interactions to ensure sufficient hole mobility.[17, 28-34] By integrating these two strategies, Nazeeruddin *et al.* prepared a new class of star-shaped D-A molecules serving as dopant-free HTMs towards ~19% PCE with enhanced device stability.[19, 35] Nonetheless, one fact is that most of reported D-A type HTMs come from relatively complicated scaffolds with multistep synthesis and purification. We recently reported a new dipolar chromophore based dopant-free HTM via a facile synthesis, which afforded a high PCE of 16.9%.[36] Following these successes, it is very crucial to exploit new D-A combinations towards high performance dopant-free HTMs with low synthetic complexity.

[a] Key Laboratory for Material Chemistry of Energy Conversion and Storage, Ministry of Education, School of Chemistry and Chemical Engineering, Huazhong University of Science and Technology, 430074, Wuhan, P. R. China .
[b] Department of Chemistry, Energy Institute and Hong Kong Branch of Chinese National Engineering Research Center for Tissue Restoration and Reconstruction, The Hong Kong University of Science and Technology, Clear Water Bay, Kowloon, Hong Kong.
[c] Institute of Polymer Optoelectronic Materials and Devices, State Key Laboratory of Luminescent Materials and Devices, South China University of Technology, 510006, Guangzhou, P. R. China.
† These authors contributed this work equally.

Electronic Supplementary Information (ESI) available: [details of any supplementary information available should be included here]. See DOI: 10.1039/x0xx00000x

View Article Online
DOI: 10.1039/C7SC05484J

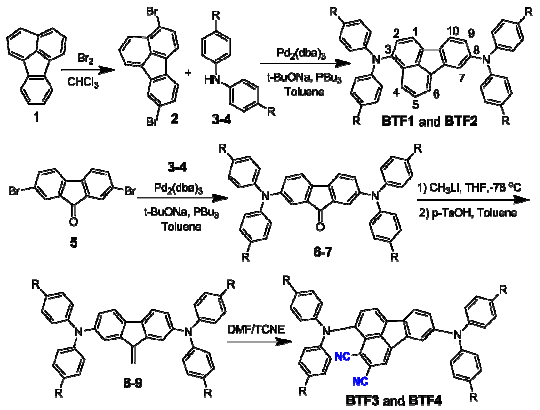

3, 6, BTF1 and BTF 3: R = -Me; 4, 7, BTF2 and BTF 4: R = -OMe

Scheme 1. Synthetic route of fluoranthene-cored HTMs (**BTF1-4**).

One of key factors for designing high performance HTMs is designing a suitable core structure. Fluoranthene is one typical cyclopentene-fused polycyclic aromatic hydrocarbon, and exhibits a rigid planarized structure that can favor to form enhanced π-π stacking. More importantly, fluoranthene, as a substructure of fullerene, shows a typical electron-deficient character due to the cyclopenta-fused nonalternant structure.[37-40] Thus, fluoranthene may be an ideal electron-withdrawing building block to construct D-A type HTMs for PVSCs, which however has not been reported possibly due to a lack of efficient molecular design strategy. In this study, we describe a new and facile synthetic method to prepare unreported 2,3-dicyano-fluoranthene moiety as efficient core towards high performance dopant-free HTMs.

Results and discussion

The synthetic route of HTMs is shown in **Scheme 1,** while the details are provided in Experimental Section in Supporting Information (SI). First, we prepared fluoranthene-cored **BTF1**-**2** via a simple Buchwald-Hartwig coupling reaction between the readily accessible 3,8-dibromo-fluoranthene (**2**)[41] and

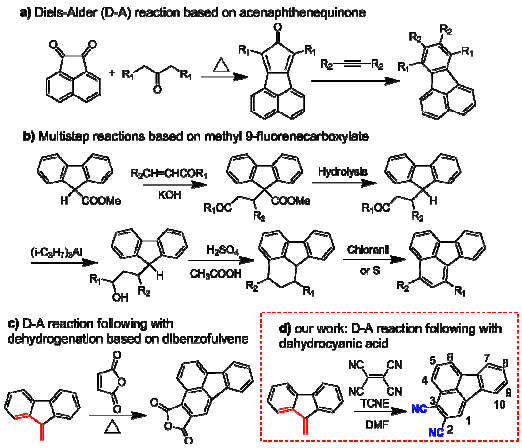

Scheme 2. Synthetic methods for functionalized fluoranthenes.

diphenylamine units (**3**-**4**). So far, facile synthesis of functionalized fluoranthene derivatives remains a challenge. One of the most widely methods of affording fluoranthenes is through typical Diels-Alder (D-A) reaction based on the acenaphthenequinone derivatives (**Scheme 2a**), but the functionalized positions of this method are always limited, mainly on C7-C10 positions.[42, 43] Another typical method proposed by Stubbs and Tucker *et al.* employs fluorene derivatives as the starting materials (**Scheme 2b**), but the total synthetic efficiency is too poor due to the tedious multistep reactions.[44]

Through a careful searching, we encouragingly found in 1949, dibenzofulvene and maleic anhydride were reported as the starting materials by Wang *et al.* to yield 2,3-substituted fluoranthene based on the D-A reaction following with dehydrogenation (**Scheme 2c**).[45] Although the yield of this reaction is low, only ~10%, the simple and facile procedure is very attractive for us. Thus, with a purpose of synthesizing more electron-deficient fluoranthene core, tetracyanoethylene (TCNE) was selected as the dienophile to react with dibenzofulvene (**Scheme 2d**) through D-A reaction but following with dehydrocyanic acid. Excitingly, 2,3-dicyano-fluoranthene was successfully obtained as we expected, in spite of with a low isolated yield of 3.5%. With an indirect method, we prepared diphenylamine moieties substituted dibenzofulvene (**8**-**9**) first, and then used them as the critical intermediates to react with TCNE as shown in **Scheme 1**, which successfully obtained our desired products, **BTF3**-**4**, with enhanced isolated yields (29.1% for **BTF3** and 43.0% for **BTF4**). The electron-rich substitutions were found to activate the reactivity of fulvene. This can be further evidenced by the higher yield of **BTF4**, as methoxyl groups in **9** make diene more electron-rich. Moreover, due to the facile synthesis, all synthetic costs, 7.1 $/g, 11.4 $/g, 53.1 $/g and 62.8 $/g for **BTF1**-**4** (**Table S1**-**S4**), respectively, are much cheaper than that of spiro-OMeTAD, making them good material candidates suitable for large scale production.

The ground-state geometric structures of **BTF3** (Triclinic, P-1 space group) and **BTF4** (Monoclinic, $P2_1/c$ space group) were refined by X-ray crystallography, and the detail data are shown in **Table S5**-**S6** in SI. **Figure 1** shows the packing arrangements of **BTF3**-**4**. According to the relative arrangement between molecules and contact positions, four types of molecular packing modes are totally found (**Figure 1a** and **S3**-**S4**), including H-type dimeric stack through dipole-dipole interactions due to dicyano-substitutions (mode 1), H-type dimeric stack through π-π interactions between two adjacent molecules (mode 2), J-type dimeric stack through π-π interactions between two adjacent diphenylamine units (mode 3), and herringbone stack through π-π interactions between two adjacent molecules (mode 4).

As shown in **Figure 1b**, **BTF3** molecules pack into highly ordered and extended H-aggregates along the (0-11) plane, wherein two types of molecular stacks (mode 1 and 2) appear in an alternating fashion. In stack mode 1, the stack distance between two dicyano-fluoranthene units is 3.515 Å, while that in stack mode 2 is 3.435 Å. Except short stack distance, the

View Article Online
DOI: 10.1039/C7SC05484J

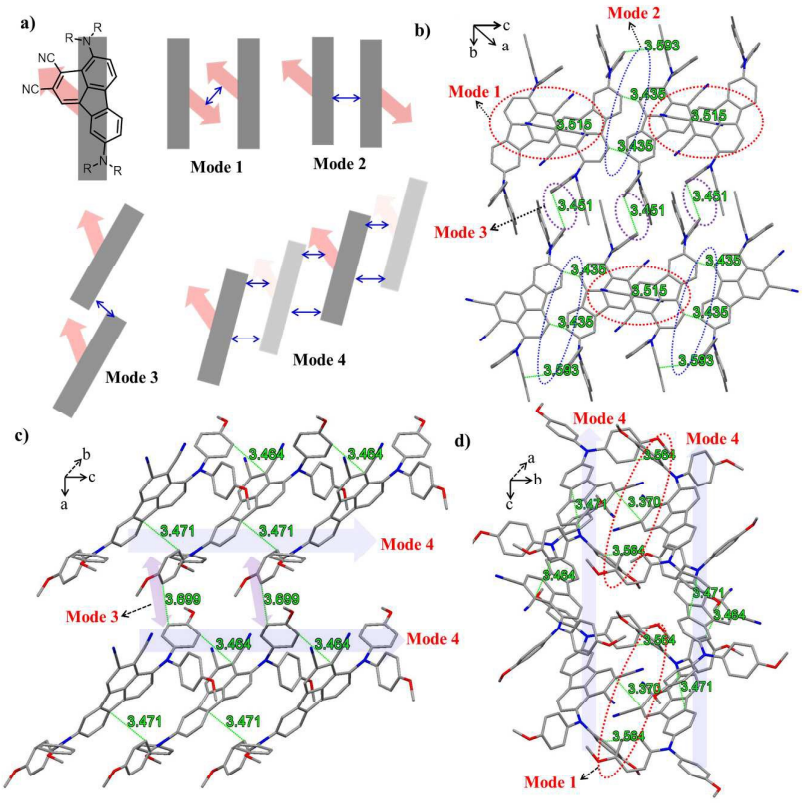

Figure 1. a) Schematic representations of the π-stack modes of **BTF3**-**4** based on single-crystal X-ray analyses, while block arrows mean the direction of dipole moments, and double arrow lines represent the positions of π-stack; b) π-stacks of **BTF3** viewed along *a* axis; c) π-stacks of **BTF4** viewed along *b* axis; d) π-stacks of **BTF4** viewed along *a* axis. For clarity, the hydrogen atoms and solvent molecules in **BTF3** are omitted. The π-stack distances are noted in green color.

contact area in mode 2 is much larger than that in mode 1, as the diphenylamine units also show a close contact with each other with a distance of 3.593 Å. Moreover, it is encouragingly found **BTF3** molecules in two adjacent H-aggregates can pack into highly ordered J-like aggregates along the (100) plane based on the stack mode 3 with a π-π-distance of 3.451Å. Thus, the solid state structure of **BTF3** can be classified as a two-dimensional "brick-wall"-like assembly.

BTF4 molecules interestingly show a highly ordered herringbone assembly with partial edge-to-face packing along the (101) plane (stack mode 4, **Figure 2c**). And due to the asymmetrical nature of cyano-fluoranthene, they contact in three different positions (**Figure S4**) with a π-π-distance of 3.464 Å, 3.471 Å, and 3.617 Å, respectively, making the molecular packing very dense. Different from those observed in **BTF3**, the neighboring herringbone assemblies interact with each other along both (110) and (101) planes, based on stack mode 3 and 1, respectively. Thus, the packing structure of **BTF4** can be classified as a quasi-three-dimensional herringbone assembly. The edge-to-face π-π-distance within dimer in stack mode 3 for **BTF4** is slightly longer (3.669 Å) than that in **BTF3**. However, a much shorter dipole-dipole interaction distance of 3.37 Å is obtained for **BTF4** in stack mode 4, attributed to that a close edge-to-face π-contact with a distance of 3.564 Å between diphenylamine units also occurs. On the contrary, we only obtained a low-quality single crystal of **BTF1** for structure analysis, which however indicates an absence of strong π-π interactions (**Figure S5**). Based on these results, we can conclude cyano-substitution plays a critical role in enabling strong intermolecular interactions in solid states, which thus are expected to be beneficial to achieve efficient charge transport.

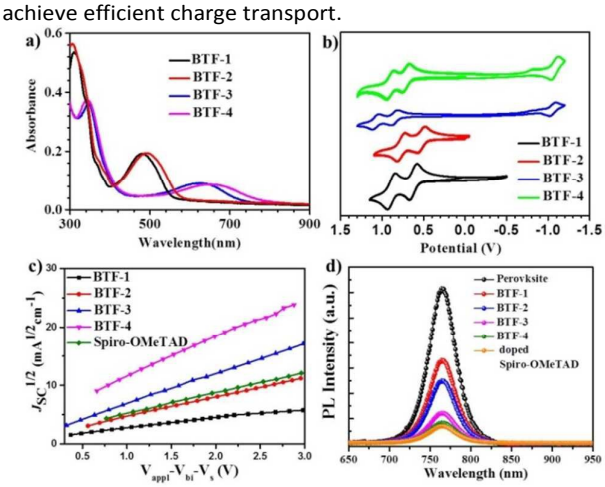

Figure 2. a) The film absorption spectra. b) The CV curves versus Fe/Fe^+ (0.66 V) measured in DCM solution. c). The hole injection characteristics measured by SCLC method based on the device structure of ITO/V_2O_5/HTMs/V_2O_5/Al. d) Steady state PL spectra of the bilayered perovskite films with or without capping different HTLs.

View Article Online
DOI: 10.1039/C7SC05484J

Table 1. Optical, electrochemical, and hole mobility properties of **BTF1-4**.

HTMs	λ_{sol} [a] (nm)	λ_{fil} [b] (nm)	E_{opt} [c] (eV)	E_{HOMO} [d] (eV)	E_{LUMO} (eV)	μ [f] ($cm^2V^{-1}s^{-1}$)
BTF1	304,475	310,481	2.24	-4.94	-2.68 [e]	1.46×10^{-5}
BTF2	305,482	308,493	2.16	-4.80	-2.59 [e]	2.13×10^{-5}
BTF3	344,609	347,629	1.70	-5.19	-3.46 [d]	6.36×10^{-5}
BTF4	344,632	344,654	1.59	-5.02	-3.38 [d]	1.17×10^{-4}

[a] Absorption maxima in DCM solutions. [b] Absorption maxima of thin films. [c] Optical band gap calculated from film absorption edges. [d] Measured from electrochemistry experiments. [e] Calculated by an equation of $E_{LUMO} = E_{HOMO}+E_{opt}$. [f] Measured by SCLC method.

The absorption spectra of **BTF1-4** in diluted solutions and as thin films are shown in **Figure S6** and **Figure 2a**, respectively, with related data listed in **Table 1**. All spectra show two distinct absorption bands, ascribed to localized π-π* transitions and intramolecular charge transfer (ICT). By comparing the film spectra with their corresponding solution spectra, it is found the low-energy absorption bands of **BTF3-4** are more red-shifted than those of **BTF1-2**, suggesting aggregation of former are more pronounced, consistent with the results from crystal structure analysis. Both methoxy- and cyano- substitutions result in a red-shift in absorption bands, while the red-shift degree for latter is much larger, up to 150 nm of absorption maximum for **BTF4**, ascribed to more effective ICT. The absorption edges of **BTF1-4** in thin films are determined to be 554, 575, 731 and 781 nm, respectively, corresponding to the optical bandgap (E_{opt}, **Table 1**) of 2.24, 2.16, 1.70, and 1.59 eV, respectively.

Their HOMO and lowest unoccupied molecular orbital (LUMO) levels were determined by cyclic voltammetry (CV), and the CV curves in DCM solutions are given in **Figure 2b**, with data summarized in **Table 1**. Both **BTF3-4** display reversible oxidative and reductive processes, while only oxidative processes observed for **BTF1-2**. The HOMO levels of **BTF1-4** are obtained as -4.94, -4.80, -5.19, and -5.02 eV, respectively, versus Fc/Fc^+. As shown, the cyano-substitution results in a decrease in HOMO levels for **BTF3-4**, making them more compatible with perovskites to facilitate hole extraction (**Figure S10** and **S17**). Moreover, we noted the introduction of electron-rich methoxy groups can induce an increase in HOMO levels. The LUMO levels of **BTF3-4** are calculated from the onset of reduction potential, -3.46 and -3.38 eV, respectively, while those of **BTF1-2** are determined as -2.68 and -2.59 eV, respectively, by subtracting E_{opt} from HOMO levels.

The hole mobilities (μ) of **BTF1-4** without adding any dopants were measured by space-charge-limited-current (SCLC) method (**Figure 2c**). As shown in **Table 1**, the μ values of **BTF3-4** are 6.36×10^{-5} and 1.17×10^{-4} $cm^2V^{-1}s^{-1}$, respectively, much higher than those of **BTF1-2** and spiro-OMeTAD (2.36×10^{-5} $cm^2V^{-1}s^{-1}$). The high mobility of **BTF4** would fulfill the needs of dopant-free HTMs. This can be attributed to its quais-three-dimensional supramolecular assembly associated with much closer molecular stacks. We also characterized the steady-state photoluminescence (PL) spectra (**Figure 2d**) of bi-layered perovskite/non-doped HTL films to check their ability of extracting holes. As seen, the PL of all bilayered films can be quenched due to the introduction of HTLs, and particularly most effectively for **BTF4**, followed by **BTF3**, **BTF2** and then **BTF1**. It is worth noting that the quenching effectiveness of dopant-free **BTF3-4** is even comparable to that of doped spiro-OMeTAD (**Figure 2d**), suggesting holes are extracted efficiently from perovskites for **BTF3-4** even without adding any dopants.

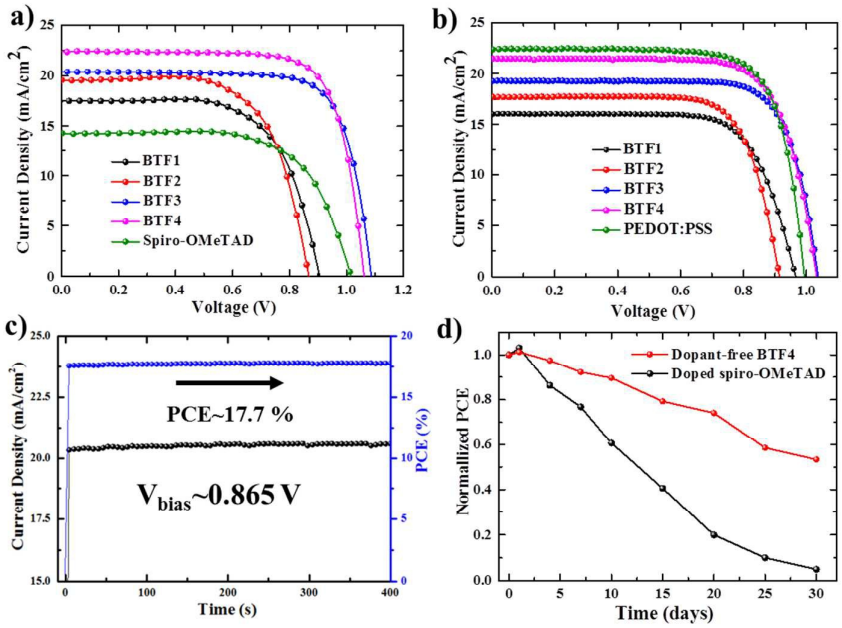

Figure 3. *J-V* curves of the best-performing conventional (a) and inverted (b) PVSCs with different dopant-free HTMs. c) Stable output current of dopant-free **BTF4** based conventional PVSC under a constant bias of 0.865 V d) The stability test of the conventional PVSCs in ambient air with a humidity of 40~50%.

View Article Online
DOI: 10.1039/C7SC05484J

Table 2. Device parameters of $(FAPbI_3)_{0.85}(MAPbBr_3)_{0.15}$-based dopant-free PVSCs using **BTF1-4**, spiro-OMeTAD and PEDOT:PSS as HTMs.

HTMs[a]	Device	V_{oc} (V)	J_{sc} (mA/cm^2)	FF (%)	PCE (%)
BTF1	n-i-p	0.91(0.90±0.01)	17.5(16.2±1.3)	62.6 (60.7±1.8)	9.97(8.84±1.12)
BTF2	n-i-p	0.85(0.84±0.02)	19.5(18.0±1.4)	63.1(60.7±2.1)	10.45(9.16±1.02)
BTF3	n-i-p	1.08(1.07±0.02)	20.4(19.2±1.1)	74.3(72.4±1.8)	16.34(15.28±1.13)
BTF4	n-i-p	1.06(1.05±0.01)	22.5(21.5±1.1)	75.6(73.7±1.9)	18.03(16.97±1.05)
Spiro-OMeTAD	n-i-p	1.02(1.01 ±0.01)	14.3(13.0±1.3)	64.0(62.4±1.5)	9.33(8.21±1.09)
BTF1	p-i-n	0.96(0.95±0.01)	16.1(14.9±1.2)	72.4(70.7±1.5)	11.19(10.02±0.98)
BTF2	p-i-n	0.91(0.90±0.02)	17.7(16.5±1.1)	74.3(72.7±1.6)	11.96(10.51±1.02)
BTF3	p-i-n	1.03(1.02 ±0.01)	19.3(18.3±1.1)	75.9(74.1±1.7)	15.09(14.14±0.96)
BTF4	p-i-n	1.03(1.01 ±0.02)	21.5(20.5±1.0)	76.8(75.3±1.5)	17.01(16.14±0.85)
PEDOT:PSS	p-i-n	0.96(0.94±0.01)	22.4(21.5±1.0)	76.4(74.7±1.6)	16.42(15.48±0.94)

We fabricated conventional n-i-p planar devices with a configuration of FTO/SnO_2/PCBM/mixed perovskite/HTL/MoO_3 /Au to evaluate the efficacy of the **BTF1-4** as dopant-free HTMs. Mixed perovskite $(FAPbI_3)_{0.85}(MAPbBr_3)_{0.15}$ (FA: NH=CHNH3$^+$; MA: CH3NH3$^+$) was used as the active light-harvesting layer. The device fabrication details are described in SI. The morphology of **BT1-4** thin films onto perovskites has been studied through scanning electron microscope (SEM), and the images are shown in **Figure S11**. As can be clearly seen, all HTLs possess smooth surface without pin-holes.

The current density-voltage (*J-V*) curves of the best-performing conventional PVSCs using dopant-free HTMs are shown in **Figure 3a**, with related photovoltaic parameters listed in **Table 2**. The champion devices based on dopant-free **BTF1** and **BTF2** showed limited PCEs of 9.97% and 10.45%, respectively, which are only slightly enhanced compared to that of spiro-OMeTAD-based dopant-free control devices (9.33%) under same fabrication conditions. By contrast, the device performance of dopant-free **BTF3-4** can be significantly improved, due to their more suitable HOMO levels and enhanced hole mobilities. The champion PVSC based on dopant-free **BTF4** delivered a very impressive PCE of 18.03% with an open-circuit voltage (V_{oc}) of 1.06, a short-circuit photocurrent (J_{sc}) of 22.5 mA cm^{-2}, and a *FF* of 75.6%, which is among best for dopant-free devices reported so far.[25] While for **BTF3**, its dopant-free devices exhibited a slightly decreased device PCE of 16.34% mainly due to a reduction in J_{sc} value caused by its inferior hole mobility compared to that of **BTF4**. To understand the charge transfer behaviors of these dopant-free HTLs, the electrochemical impedance spectroscopy (EIS) of fabricated cells was further measured at open circuit with a frequency ranging from 1 Hz to 1 MHz, and the Nyquist plots are shown in **Figure S14**. Similar to hole mobility, the obtained recombination reisistance (R_{rec}) also manifests an order of R_{rec}(**BTF4**) > R_{rec}(**BTF3**) > R_{rec}(**BTF2**)~R_{rec}(**spiro-OMeTAD**) > R_{rec}(**BTF1**). This therefore suggests **BTF3** and **BTF4** can efficiently reduce the recombination process with higher recombination resistance to produce higher FFs.

Doped conventional devices were also fabricated through using Li-TFSI as the dopant with additive of 4-tert-butyl pyridine (TBP). As shown in **Figure S16**, the device PCEs of doped **BTF1-2** can be enhanced by 40% due to an effective improvement on both V_{oc} and *FF*. Nonetheless, such enhancement is still poor by comparison with that of doped sipro-OMeTAD (18.8%). A slight enhancement on PCEs was observed for the doped **BTF3-4** based devices, while the highest PCE of 18.94% was yielded for **BTF4**. These results, on the other hand, suggest our dicyano-fluoranthene-cored molecules can serve as highly efficient HTMs without needing dopants.

Today, most HTMs used in inverted p-i-n devices are those polymer HTMs such as poly(3,4-ethylenedioxythiophene) polystyrenesulfonate (PEDOT:PSS) and polytriarylamine (PTAA).[46-49] Doping process is also required for PTAA to improve device performance.[50] PEDOT:PSS belongs to a class of self-doped polymers, however, it always suffers a large potential loss and inherent acidity-induced stability problem.[51, 52].Therefore, it is also important to develop dopant-free HTMs suitable for inverted PVSCs.[53, 54] But less molecular HTMs have been reported to be applied on both conventional and inverted planar PVSCs. In this end, inverted PVSCs with a configuration of ITO/HTL/mixed perovskite/PCBM/LiF/Ag were also tested using **BTF1-4** as the dopant-free HTMs, while PEDOT:PSS-based control device was fabricated for comparison. The *J-V* curves of best-performing devices are shown in **Figure 3b**. From **BTF1** to **BTF4,** the resulting PCEs of inverted devices increase gradually (**Table 2**), similar trend as that observed in conventional devices. The champion PCE from **BTF4**-based inverted PVSCs is 17.01%, higher than that of PEDOT:PSS-based control device (16.42%).

The stabilized PCE and photocurrent of champion devices of **BTF4** near the maximum power point (**Figure 3c and S18b**) were tested to evaluate the efficacy of *J-V* curves. The results clearly manifest the high reliability of our *J-V* curve with an absence of current hysteresis, when combing with those *J-V* curves with forward and reverse scanning direction at different scan rates (**Figure S12b and S18c**). We also measured the incident photon-to-electron conversion efficiency (IPCE) spectra of all champion conventional and inverted devices based on dopant-free **BTF1-4** (**Figure S15 and S20**), wherein the integrated J_{SC} values is consistent with those obtained from the experimental *J-V* measurements (**Table 2**).

To check if removing doping process can improve device stability of PVSCs over doped spiro-OMeTAD, we compared the environmental stability of PVSCs derived from dopant-free **BTF4** and doped spiro-OMeTAD without encapsulation. The PCE decay curves are presented in **Figure 3d**, wherein it is easily seen the performance of both devices decreased quickly

View Article Online
DOI: 10.1039/C7SC05484J

at the beginning when being stored in ambient air under a relative humidity of 40~50%. However, dopant-free **BTF4** based device can still retain over 50% of its original PCE after stored for 30 days, while the PCE of the doped spiro-OMeTAD based device almost vanished. Moreover, **BTF4**-based inverted devices also showed an enhanced stability and can retain 55% of its original PCE after being stored in air for 7 days, while 90% of PCE of PEDOT:PSS-based control device was lost (**Figure S18e**). Thus, our designed fluoranthene-cored dopant-free HTMs not only deliver a high PCE comparable to doped spiro-OMeTAD, but also show an enhanced device stability, suggesting they are very promising material candidates towards efficient PVSCs.

Conclusions

In summary, 2,3-dicyano-fluoranthene is first prepared through a new and facile synthetic method based on Diels-Alder reaction. We find fluoranthene could be an ideal building block for designing D-A type dopant-free HTMs with low synthetic cost and compatible energy levels with perovskites through rational molecular design. The detailed crystal structure analysis indicates the resulting molecules with dicyano-substituted fluoranthene as the core present highly ordered and strong molecular packing in solid states, and in particular, **BTF4** forms a quasi-three-dimensional herringbone assembly, leading to a much higher hole mobility up to 10^{-4} $cm^2V^{-1}s^{-1}$ than that of spiro-OMeTAD. Encouragingly, our designed molecules can be applied on planar PVSCs as efficient dopant-free HTMs yielding high device performance, including efficiency and stability. For **BTF4**, impressive PCEs of 18.03% and 17.01% have been achieved for conventional and inverted cells, respectively. Therefore, our work not only develops a general material design-strategy to achieve efficient dopant-free HTMs for PVSCs, but also provides a new synthetic method to obtain functionalized fluoranthenes.

Acknowledgements

This work is funded by National Science Foundation of China (Grant No. 21704030). Z. Li and H-L. Yip thank the financial support from the National 1000 Young Talents Program hosted by China. We would like to thank the Analytical and Testing Center and Research Core Facilities for Life Science in HUST for using their facilities. Dr. Xianggao Meng (Central China Normal University) is also appreciated for his help on X-ray structure refinement.

Notes and references

1. M. A. Green, A. Ho-Baillie and H. J. Snaith, *Nat. Photonics*, 2014, **8**, 506-514.
2. S. T. Williams, A. Rajagopal, C. C. Chueh and A. K. Jen, *J. Phys. Chem. Lett.*, 2016, **7**, 811-819.
3. L. Meng, J. You, T.-F. Guo and Y. Yang, *Acc. Chem. Res.*, 2016, **49**, 155-165.
4. P. Docampo and T. Bein, *Acc. Chem. Res.*, 2016, **49**, 339-346.
5. Z. Yu and L. Sun, *Adv. Energy Mater.*, 2015, **5**, 1500213.
6. https://www.nrel.gov/pv/assets/images/efficiency-chart.png.
7. J. Seo, J. H. Noh and S. I. Seok, *Acc. Chem. Res.*, 2016, **49**, 562-572.
8. C.-C. Chueh, C.-Z. Li and A. K. Y. Jen, *Energy Environ. Sci.*, 2015, **8**, 1160-1189.
9. S. Ameen, M. A. Rub, S. A. Kosa, K. A. Alamry, M. S. Akhtar, H. S. Shin, H. K. Seo, A. M. Asiri and M. K. Nazeeruddin, *ChemSusChem*, 2016, **9**, 10-27.
10. J. Shi, X. Xu, D. Li and Q. Meng, *Small*, 2015, **11**, 2472-2486.
11. H. Kim, K.-G. Lim and T.-W. Lee, *Energy Environ. Sci.*, 2016, **9**, 12-30.
12. K. Rakstys, M. Saliba, P. Gao, P. Gratia, E. Kamarauskas, S. Paek, V. Jankauskas and M. K. Nazeeruddin, *Angew. Chem. Int. Ed.* , 2016, **55**, 7464-7468.
13. B. Xu, D. Bi, Y. Hua, P. Liu, M. Cheng, M. Grätzel, L. Kloo, A. Hagfeldt and L. Sun, *Energy Environ. Sci.*, 2016, **9**, 873-877.
14. A. Molina-Ontoria, I. Zimmermann, I. Garcia-Benito, P. Gratia, C. Roldan-Carmona, S. Aghazada, M. Graetzel, M. K. Nazeeruddin and N. Martin, *Angew. Chem., Int. Ed.*, 2016, **55**, 6270-6274.
15. I. Zimmermann, J. Urieta-Mora, P. Gratia, J. Aragó, G. Grancini, A. Molina-Ontoria, E. Ortí, N. Martín and M. K. Nazeeruddin, *Adv. Energy Mater.*, 2017, **7**, 1601674.
16. I. García-Benito, I. Zimmermann, J. Urieta-Mora, J. Aragó, A. Molina-Ontoria, E. Ortí, N. Martín and M. K. Nazeeruddin, *J. Mater. Chem. A*, 2017, **5**, 8317-8324.
17. Y. Liu, Z. Hong, Q. Chen, H. Chen, W. H. Chang, Y. M. Yang, T. B. Song and Y. Yang, *Adv. Mater.*, 2016, **28**, 440-446.
18. S. Kazim, F. J. Ramos, P. Gao, M. K. Nazeeruddin, M. Grätzel and S. Ahmad, *Energy Environ. Sci.*, 2015, **8**, 1816-1823.
19. S. Paek, P. Qin, Y. Lee, K. T. Cho, P. Gao, G. Grancini, E. Oveisi, P. Gratia, K. Rakstys, S. A. Al-Muhtaseb, C. Ludwig, J. Ko and M. K. Nazeeruddin, *Adv. Mater.*, 2017, **29**, 1606555.
20. P. Qin, H. Kast, M. K. Nazeeruddin, S. M. Zakeeruddin, A. Mishra, P. Bäuerle and M. Grätzel, *Energy Environ. Sci.*, 2014, **7**, 2981-2985.
21. P. Qin, S. Paek, M. I. Dar, N. Pellet, J. Ko, M. Gratzel and M. K. Nazeeruddin, *J. Am. Chem. Soc.*, 2014, **136**, 8516-8519.
22. M. Cheng, Y. Li, M. Safdari, C. Chen, P. Liu, L. Kloo and L. Sun, *Adv.Energy Mater.*, 2017, **7**, 1602556.
23. M. Cheng, B. Xu, C. Chen, X. Yang, F. Zhang, Q. Tan, Y. Hua, L. Kloo and L. Sun, *Adv. Energy Mater.*, 2015, **5**, 1401720.
24. M. Cheng, C. Chen, X. Yang, J. Huang, F. Zhang, B. Xu and L. Sun, *Chem. Mater.*, 2015, **27**, 1808-1814.
25. X. Sun, D. Zhao and Z. Li, *Chin. Chem. Lett.*, 2017, DOI: 10.1016/j.cclet.2017.09.038.
26. Y. Wang, Z. Zhu, C.-C. Chueh, A. K. Y. Jen and Y. Chi, *Adv. Energy Mater.*, 2017, **7**, 1700823.
27. L. Cali, S. Kazim, M. Graetzel and S. Ahmad, *Angew. Chem., Int. Ed.*, 2016, **55**, 2-26.
28. C. Chen, M. Cheng, P. Liu, J. Gao, L. Kloo and L. Sun, *Nano Energy*, 2016, **23**, 40-49.
29. M. Cheng, K. Aitola, C. Chen, F. Zhang, P. Liu, K. Sveinbjörnsson, Y. Hua, L. Kloo, G. Boschloo and L. Sun, *Nano Energy*, 2016, **30**, 387-397.
30. Y. Liu, Q. Chen, H.-S. Duan, H. Zhou, Y. Yang, H. Chen, S. Luo, T.-B. Song, L. Dou, Z. Hong and Y. Yang, *J. Mater. Chem. A*, 2015, **3**, 11940-11947.

View Article Online
DOI: 10.1039/C7SC05484J

31. J. H. Yun, S. Park, J. H. Heo, H.-S. Lee, S. Yoon, J. Kang, S. H. Im, H. Kim, W. Lee, B. Kim, M. J. Ko, D. S. Chung and H. J. Son, *Chem. Sci.*, 2016, **7**, 6649-6661.
32. F. Zhang, C. Yi, P. Wei, X. Bi, J. Luo, G. Jacopin, S. Wang, X. Li, Y. Xiao, S. M. Zakeeruddin and M. Grätzel, *Adv. Energy Mater.*, 2016, **6**, 1600401.
33. G.-W. Kim, J. Lee, G. Kang, T. Kim and T. Park, *Adv. Energy Mater.*, 2017, DOI: 10.1002/aenm.201701935.
34. J. Lee, M. Malekshahi Byranvand, G. Kang, S. Y. Son, S. Song, G. W. Kim and T. Park, *J. Am. Chem. Soc.*, 2017, **139**, 12175-12181.
35. K. Rakstys, S. Paek, P. Gao, P. Gratia, T. Marszalek, G. Grancini, K. T. Cho, K. Genevicius, V. Jankauskas, W. Pisula and M. K. Nazeeruddin, *J. Mater. Chem. A*, 2017, **5**, 7811-7815.
36. Z. Li, Z. Zhu, C. C. Chueh, S. B. Jo, J. Luo, S. H. Jang and A. K. Jen, *J. Am. Chem. Soc.*, 2016, **138**, 11833-11839.
37. Y. Zhou, L. Ding, K. Shi, Y. Z. Dai, N. Ai, J. Wang and J. Pei, *Adv. Mater.*, 2012, **24**, 957-961.
38. S. Kumar and S. Patil, *J. Phys. Chem. C*, 2015, **119**, 19297-19304.
39. Y. Q. Zheng, Y. Z. Dai, Y. Zhou, J. Y. Wang and J. Pei, *Chem.Commun.*, 2014, **50**, 1591-1594.
40. A. Palmaerts, M. V. Haren, L. Lutsen, T. J. Cleij and D. Vanderzande, *Macromolecules*, 2006, **39**, 2438-2440.
41. W. Wu; and W. Gao, 2016, DOI: US 2016/0268514 A1.
42. Y. Yuan, G. Q. Zhang, F. Lu, Q. X. Tong, Q. D. Yang, H. W. Mo, T. W. Ng, M. F. Lo, Z. Q. Guo, C. Wu and C. S. Lee, *Chem. Asian J.*, 2013, **8**, 1253-1258.
43. C. M. Thompson, G. Occhialini, G. T. McCandless, S. B. Alahakoon, V. Cameron, S. O. Nielsen and R. A. Smaldone, *J. Am. Chem. Soc.*, 2017, **139**, 10506-10513.
44. H. W. D. Stubbs and S. H. Tucker, *J. Chem. Soc.*, 1950, 3288-3292.
45. N. Campbell and H. Wang, *J. Chem. Soc.*, 1949, 1513-1515.
46. J. H. Heo, H. J. Han, D. Kim, T. K. Ahn and S. H. Im, *Energy Environ. Sci.*, 2015, **8**, 1602-1608.
47. W. S. Yang, J. H. Noh, N. J. Jeon, Y. C. Kim, S. Ryu, J. Seo and S. I. Seok, *Science*, 2015, **348**, 1234-1237.
48. W. Yan, S. Ye, Y. Li, W. Sun, H. Rao, Z. Liu, Z. Bian and C. Huang, *Adv. Energy Mater.*, 2016, **6**, 1600474.
49. E. Edri, S. Kirmayer, D. Cahen and G. Hodes, *J. Phys. Chem. Letter.*, 2013, **4**, 897-902.
50. Q. Wang, C. Bi and J. Huang, *Nano Energy*, 2015, **15**, 275-280.
51. Q. Xue, G. Chen, M. Liu, J. Xiao, Z. Chen, Z. Hu, X.-F. Jiang, B. Zhang, F. Huang, W. Yang, H.-L. Yip and Y. Cao, *Adv. Energy Mater.*, 2016, **6**, 1502021.
52. K.-G. Lim, S. Ahn, Y.-H. Kim, Y. Qi and T.-W. Lee, *Energy Environ. Sci.*, 2016, **9**, 932-939.
53. C. Huang, W. Fu, C. Z. Li, Z. Zhang, W. Qiu, M. Shi, P. Heremans, A. K. Jen and H. Chen, *J. Am. Chem. Soc.*, 2016, **138**, 2528-2531.
54. H. Chen, W. Fu, C. Huang, Z. Zhang, S. Li, F. Ding, M. Shi, C.-Z. Li, A. K. Y. Jen and H. Chen, *Adv. Energy Mater.*, 2017, **7**, 1700012.

View Article Online
DOI: 10.1039/C7SC05484J

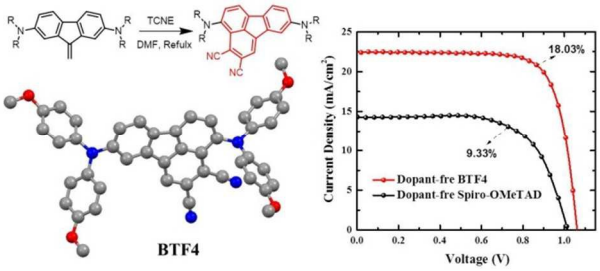

Unreported 2,3-dicyano-fluoranthene was first prepared as an efficient electron-withdrawing building block for constructing D-A type dopant-free hole transporting materials.